Colloids and Surfaces B: Biointerfaces 135 (2015) 309–315

Contents lists available at ScienceDirect

Colloids and Surfaces B: Biointerfaces

journal homepage: www.elsevier.com/locate/colsurfb

# Robust fluorescence sensing platform for detection of CD44 cells based on graphene oxide/gold nanoparticles

Ha Young Jeong, Seung Hun Baek, Sung-Jin Chang, Seon Ah Cheon, Tae Jung Park*

*Department of Chemistry, Chung-Ang University, 84 Heukseok-ro, Dongjak-gu, Seoul 156-756, Republic of Korea*

ARTICLE INFO

*Article history:*
Received 2 June 2015
Received in revised form 4 July 2015
Accepted 30 July 2015
Available online 1 August 2015

*Keywords:*
Graphene oxide/gold nanoparticles (GO/AuNPs)
Fluorescence sensing
Signal-to-background ratio enhancer
Aptamer
Hyaluronic acid binding domain of CD44

ABSTRACT

Gold-coated graphene oxide hybrid material (GO/AuNPs) has exceptional physical and chemical properties like π–π stacking interaction and plays a role in quencher of fluorescence dye. Therefore, GO/AuNPs could enhance the signal-to-background ratio with fluorescence dye that was the point in this fluorescent biosensor. In this study, tetramethyl-6-carboxy-rhodamine (TAMRA)-labeled aptamers that specifically interact with the hyaluronic acid binding domain of CD44 were used as targets to investigate the applicability of the method. GO/AuNPs–TAMRA-aptamer complexes could detect CD44 target cancer cells within a concentration range of $1 \times 10^1$ to $1 \times 10^7$ CFU/mL. A linear relationship was observed between target cell concentration and relative fluorescence intensity. The more mounted up CD44 target cell concentrations, relative fluorescence intensity of GO/AuNPs–TAMRA-aptamer complexes was increased even more, which was superior to that of GO alone. Sensitivity of the detection system displayed a low detection limit of $1 \times 10^1$ CFU/mL. Additionally, this method is specific in that fluorescence is not much enhanced in CD44 negative cancer cell line. Thus, the fluorescence sensing based on GO/AuNPs could be developed to receptive and robust detection tool for various target molecules.



## 1. Introduction

In recent decades, research and development of DNA biosensors has attracted considerable attention in the fields of clinical diagnosis, screening for food poisoning, and environmental monitoring [1–3]. As a result, numerous types and techniques of DNA biosensors based on fluorescence, colorimetry, electrochemistry, and surface plasmon resonance spectroscopy have been investigated and developed for DNA detection [4–9]. For example, fluorescence-based DNA biosensors exhibit relative ease of operation, high specificity and sensitivity, as well as high-throughput analysis [10–13]. Despite of these advantages, a low signal-to-background ratio may occur due to the intrinsic signal of fluorescence dyes in the absence of targets [14]. Therefore, there is a need for a fluorescence-based DNA biosensor that eliminates the high background while maintaining target specificity.

Recently, nanomaterials have been used in the field of biosensor systems. Especially, graphene oxide (GO) has various interesting features like as large surface area, volume ratio, and quenching effect by surface energy transfer with fluorescence dyes [15–18]. Moreover, GO offers abundant carboxyl, hydroxyl, and epoxy groups on the surface of a two-dimensional layered carbon sheet from a graphene precursor [19]. It can provide unique characteristics such as via π–π stacking and weak electrostatic attractions between single-stranded DNA (ssDNA) and the GO surface [20,21]. This is a key factor of enhancing the sensitivity of fluorescence-based DNA detection system. In spite of their merits and capabilities of GOs, however, serious level of agglomeration may reduce their surface area and stability. Consequently, these phenomena limit the interaction between GO and ssDNA [22,23].

To overcome such problems, hybrid nanomaterial has been provided an alternative choice to meet the requirements. Hybrid materials with nanoparticles such as silica, silver, and platinum as coating materials have been used on the surface of GO [24–26]. However, these nanoparticles are inappropriate for DNA-based biosensor because of repulsive force or high reactivity with other reagents [27–29]. Conversely, AuNPs have many outstanding properties including biocompatibility, chemical inertness, ability to immobilize the ssDNA and enhancement of solubility [30,31]. Therefore, combining of the AuNPs onto the surface of GO (GO/AuNPs) can improve the stability in solution and maintain a certain distance from GO. Moreover, GO/AuNPs allows higher quenching efficiency than GO or AuNPs alone that can provide a good signal-to-background ratio for improving the performance of fluorescent methods [32–35].

* Corresponding author. Fax: +82 2 825 4736.
*E-mail address:* tjpark@cau.ac.kr (T.J. Park).

http://dx.doi.org/10.1016/j.colsurfb.2015.07.083
0927-7765/

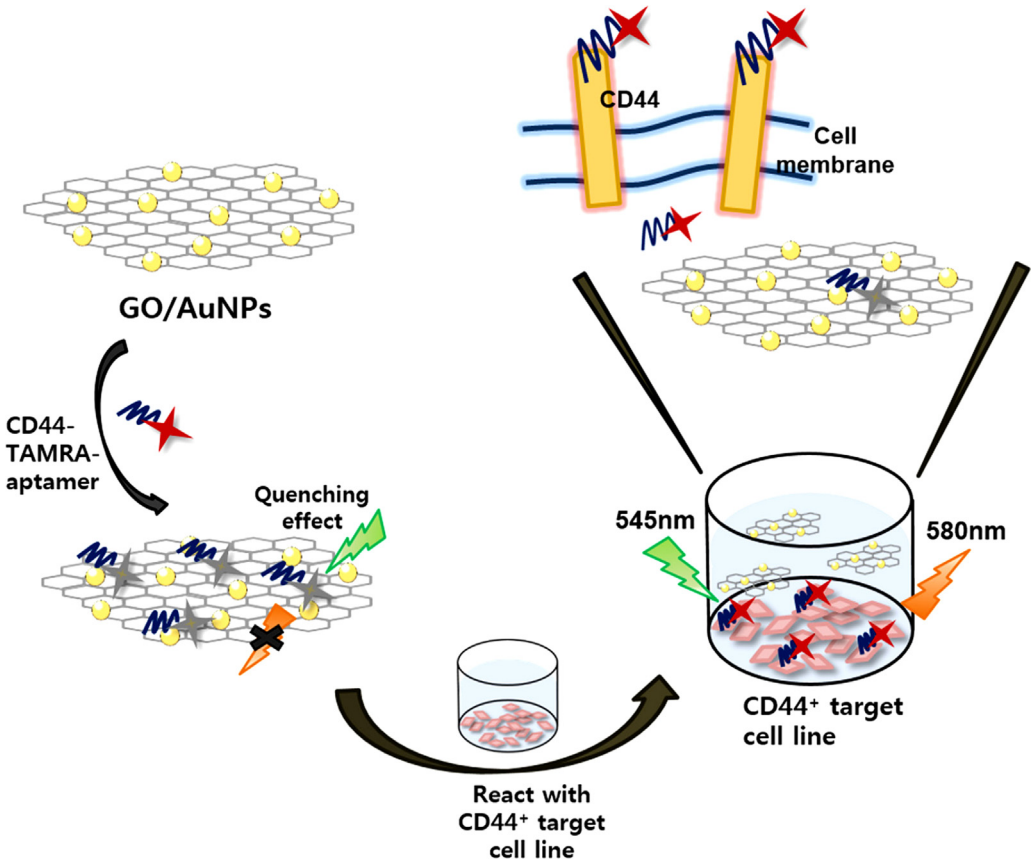


**Fig. 1.** Schematic illustration of GO/AuNPs sensing-based fluorescent detection.

The integral transmembrane protein CD44 is the primary receptor for hyaluronic acid (HA). It promotes proliferation, migration, invasion, and tumor-associated angiogenesis, which result in cancer development [36]. CD44 can therefore be used as a biomarker for cancer diagnosis or prevention. Conjugation of chemotherapeutic drugs or other anticancer agents to HA or anti-CD44 antibodies has demonstrated for successful delivery to the tumor site as well as increased efficacy in animal tumor models. This suggests that inhibition of tumor growth and metastasis occurred by CD44–HA interactions, thus indicating that these interactions may provide a new approach to the targeted diagnosis and treatment of specific cancers [36–38]. However, this hypothesis is difficult to evaluate because the interaction between HA and CD44 is very weak. Aptamer has become increasingly important diagnostic and therapeutic molecular tools [39] and an aptamer that specifically binds to the HA-binding domain of CD44 with high affinity was reported [37,40].

Here, we describe a simple and sensitive fluorescence-sensing platform based on GO/AuNPs, which constructs for fluorescence detection of CD44 with CD44-specific aptamer (Fig. 1). Initially, tetramethyl-6-carboxyrhodamine (TAMRA) dye-labeled CD44 aptamer strongly binds to the surface of GO/AuNPs to form a self-assembled structure via π–π stacking and electrostatic attractions. Accordingly, the fluorescence of TAMRA dye has almost perfectly quenched. When GO/AuNPs–aptamer complexes add to target cell lines, hybridization occurs between the CD44 aptamer and HA-binding domain of $CD44^+$ target cells. Finally, the fluorescence intensity of TAMRA markedly increases by its release from the GO/AuNPs surface compared with GO alone. This fluorescence-sensing platform based on GO/AuNPs can be adapted to provide accurate, sensitive, and specific detection of diverse targets, and serve as a signal-to-background ratio enhancer with improved efficacy compared to GO alone.

## 2. Materials and methods

### 2.1. Reagents and apparatus

Graphite powder was obtained from Kanto Chemical (Kanto, Japan). Potassium permanganate ($KMnO_4$), phosphorus pentoxide ($P_2O_5$), concentrated sulfuric acid ($H_2SO_4$), potassium persulfate ($K_2S_2O_8$), gold(III) chloride trihydrate ($HAuCl_4{\cdot}3H_2O$), trisodium citrate ($Na_3C_6H_5O_7$), and phosphate-buffered saline (pH 7.4) were purchased from Sigma–Aldrich (St. Louis, MO). Hydrazine solution ($NH_2NH_2$), hydrochloric acid (HCl), and hydrogen peroxide ($H_2O_2$) were obtained from Samchun (Seoul, Korea). Trypsin-EDTA solution was purchased from Welgene (Gyeongsan, Korea). Filter papers were purchased from Whatman (Dassel, Germany). The TAMRA-labeled aptamer (5′-TAMRA-GAG ATT CAT CAC GCG CAT AGT CCC AAG GCC TGC AAG GGA ACC AAG GAC ACA GCG ACT ATG CGA TGA TGT CTT C-3′) was synthesized by MACROGEN (Seoul, Korea). Five types of human cancer cell lines (SKOV3, MDA-MB-231, A549, MCF-7, and T98G) were obtained from Korean Cell Line Bank (Seoul, Korea). All other reagents were analytical reagent grade and were used as received without further purification or treatment. Ultrapure water obtained from a Millipore water purification system (Milli-Q, Billerica, MA) was used in all assays. UV/vis spectrophotometer analysis was conducted with OPTIZEN POP spectroscopy (Mecasys, Daejeon, Korea). Fluorescence spectroscopic analysis was performed using the OLYMPUS DP73 microscope (Tokyo, Japan) and transmission electron microscope (TEM) analysis was conducted with a Tecnai G2 F30 S-Twin microscope (FEI, Hillsboro, OR). Atomic force microscope (AFM,

Park Systems, Suwon, Korea) characterizations were conducted with non-contact mode on an XE-100 instruments at a scanning rate of 1 Hz and operated by XEP software.

### 2.2. Synthesis of GO/AuNPs

#### 2.2.1. Preparation of graphene oxide (GO)

GO was prepared from graphite powder using a modified Hummers' method [41,42]. Graphite powder (2 g) was mixed with a solution of 50 wt% $H_2SO_4$ (27 mL), $K_2S_2O_8$ (2 g), and $P_2O_5$ (2 g) at 85 °C, and the mixture was stirred for 5 h. The solution was then cooled to room temperature and added to 500 mL of deionized (DI) water. This mixture was stirred overnight, and then dried at room temperature after filtering. The dried and peroxidized graphite were added to a cooled solution of 50 wt% $H_2SO_4$ (270 mL). $KMnO_4$ (10 g) was slowly added in ice bath system with stirring for 1 h and reacted at room temperature for 24 h. 500 mL of DI water was later added, followed by the addition of 20 mL 30% $H_2O_2$. In this step, the color of the solution was changed from dark brown to yellow. The mixture was then washed and filtered with an aqueous solution of 10 wt% HCl (1 L) and DI water (1 L) to remove unreacted ions. The yellow products were dried at 60 °C.

#### 2.2.2. Synthesis of gold-coated GO

The synthesis of GO/AuNPs composites was based on the reduction of the Au(III) complex by sodium citrate. First, 5 mL of the graphene oxide solution (1.5 mg/mL) was added to a solution of $HAuCl_4$ (0.095 g/mL, 100 mL), which was then sonicated for 30 min to promote interaction of the gold ions on the GO surfaces. The reaction solution was heated to 80 °C following dropwise addition of a sodium citrate (0.85 mol/L, 1.92 mL) solution. The reaction was allowed to continue for 1 h. The resulting solution was then centrifuged at 842 × *g* for 10 min and washed several times with distilled water to remove free AuNPs. Finally, the nano-composites were dried at 60 °C.

### 2.3. Cell culture

The SKOV3 ovarian cancer cells, MDA-MB-231 breast cancer cells, and A549 lung cancer cells were maintained in RPMI-1640 medium (GenDEPOT, Barker, TX) supplemented with 10% fetal bovine serum (FBS) and 1X antibiotic-antimycotic solution. The MCF-7 breast cancer cells and T98G brain cancer cells were maintained in Dulbecco's modified Eagle's medium (DMEM, GenDEPOT, Barker, TX) supplemented with 10% FBS and 1X antibiotic-antimycotic solution. Cells were cultured on 24-well plates prior to fluorescence experiments with 5% $CO_2$ at 37 °C.

### 2.4. Cell viability assay

The cell viability was evaluated by MTT assay. SKOV3 and MCF-7 cells of $1 \times 10^3$ CFU/well were seeded in 96 well plates and incubated with 5% $CO_2$ gas at 37 °C for 36 h, respectively. The cells were then treated with different concentrations of GO/AuNPs at 37 °C under 5% $CO_2$. After 24 h, the cells were incubated with 100 μL of 0.5 mg/mL thiazolyl blue tetrazolium bromide (MTT, Sigma–Aldrich) in PBS solution for 3 h at 37 °C under 5% $CO_2$. Finally, the MTT solution was removed and the produced formazan crystals were dissolved in 100 μL of dimethyl sulfoxide (DMSO, Sigma–Aldrich) for 25 min. Optical density of formazan solution was monitored at 540 nm using Synergy H1 Hybrid Reader from BioTek (Winooski, VT).

### 2.5. Fluorescence detection

The TAMRA-aptamer, specific for the HA-binding domain of CD44, was suspended in PBS solution (20 mM, pH 7.4) and 1 μL of 20 nM aptamer was mixed with 18 μL of 1 mg/mL of GO or GO/AuNPs in a 1.5 mL tube. This mixture was allowed to react for 15 min and then centrifuged at 842 × *g* for 10 min. The resulting pellet was separated from the supernatant. The pellet was resuspended with PBS solution after discarding the supernatant. The TAMRA-aptamer-GO or -GO/AuNPs solution was mixed with target cells at various concentrations ranging from $1 \times 10^1$ to $1 \times 10^7$ CFU/mL in 24-well plates in the final volume of 500 μL, and incubated for 1 h at 37 °C. After treatment, the cells were washed twice with PBS solution to exclude the possibility that remaining particles can affect the fluorescence detection. Then, all fluorescence measurements were performed using Synerge H1 Hybrid multiplate Reader. The excitation wavelength was 545 nm and emission spectra were collected at 580 nm. Experiments for the optimization of sensing conditions were carried out under identical conditions and were repeated three times.

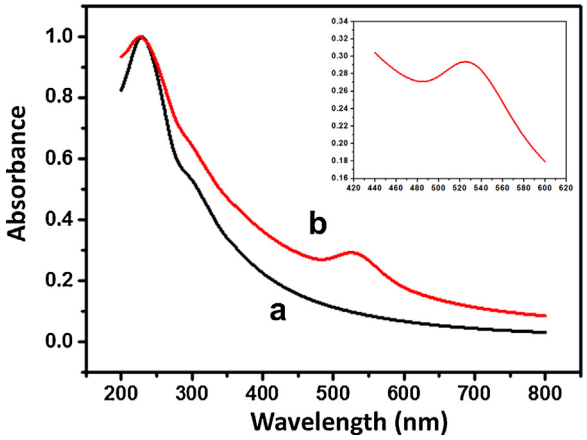


**Fig. 2.** UV–vis absorption spectra of (a) GO and (b) GO/AuNPs. Inset: UV–vis absorption spectra obtained for the gold nanoparticles of synthesized GO/AuNPs at 525 nm.

### 2.6. Flow cytometric analysis

$CD44^+$ SKOV3 and $CD44^-$ MCF-7 cells were incubated with GO and GO/AuNPs–TAMRA-aptamer complexes for 1 h at 37 °C, respectively. The cells were then collected using trypsin-EDTA solution, and centrifuged at 842 × *g* for 4 min. The cell pellet was washed twice with PBS solution (20 mM, pH 7.4), and flow cytometric analysis was performed on the BD Accuri C6 flow cytometer (BD Bioscience, San Jose, CA).

## 3. Results and discussion

### 3.1. Characterization of graphene oxide/gold nanoparticles

We prepared GO and GO/AuNPs sheets based on the Hummers' method [41,42] and UV–vis absorption spectra of the synthesized GO and GO/AuNPs nanocomposites was confirmed (Fig. 2). A peak at 230 nm in the GO absorbance spectrum represented the transition of aromatic CC bond of the GO. The shoulder peak at 300 nm was correspond to transition of C=O bond now embedded by exfoliation and intercalation on the graphite [43]. Then, GO/AuNPs were formed by redox reactions of the $HAuCl_4$ *in situ* on the partially GO surface. Thus, appearance of the bands at 525 nm of the UV–vis region was attributed to the formation of AuNPs on the GO sheets. However, the absorption peak at 300 nm of GO/AuNPs may be decreased because of electrostatic interaction between GO and gold ions [44].

TEM images and AFM analysis were examined for the GO/AuNPs before the addition of TAMRA-aptamer (Fig. 3). The GO sheets were

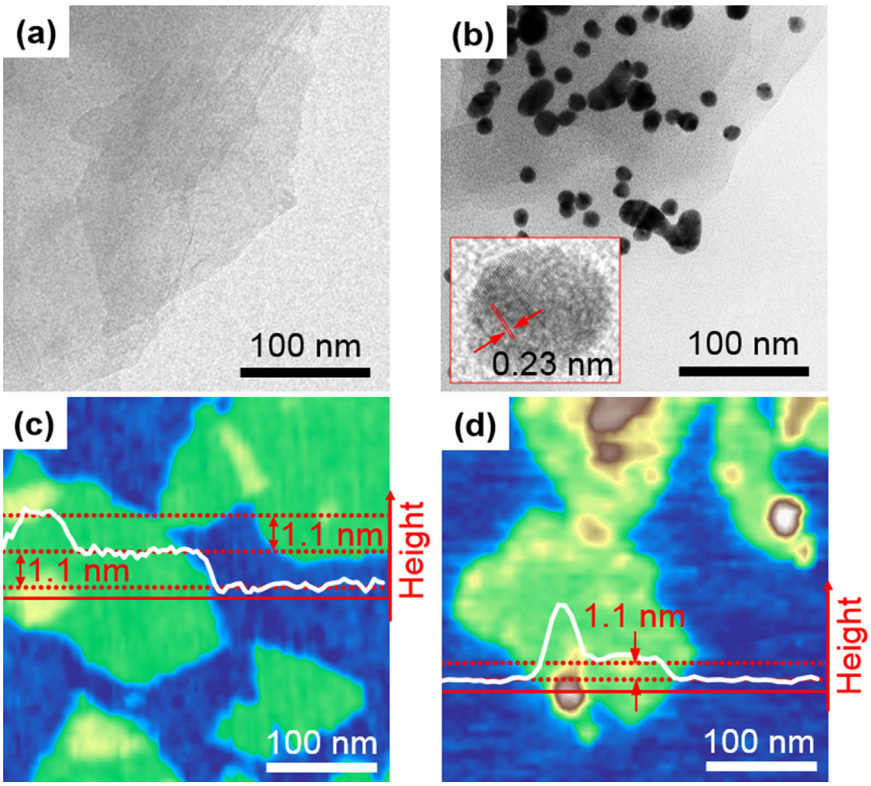


**Fig. 3.** Representative TEM images of (A) GO and (B) GO/AuNPs. AFM images and height profiles of the (C) GO and (D) GO/AuNPs: concentration of AuNPs was 0.85 M.

very thin, consisting of one to several layers and the broad and flat GO surface can provide a large surface area for loading AuNPs. A TEM image of GO/AuNPs reveals that the AuNPs randomly dispersed on the GO sheets, with an average size of 15.2 nm and the interplanar distances was 0.23 nm. This finding indicates that Au nuclei are randomly formed only on the GO sheets and subsequently grown for a given thermal reduction time. AFM analysis was carried out to determine the topographical shape for each step during the production of GO/AuNPs-aptamers. The average thickness of GO sheets was approximately 1.1 nm, and some parts of GO/AuNPs sheets was equivalent size to those of the individual GO sheets. When AuNPs were absorbed on the GO surface, the height was in the range between 6 and 10 nm which is similar size to that of AuNPs from TEM images. These results confirmed that single GO layers can provided as substrates to load a number of AuNPs.

The fluorescence quenching efficiency of GO/AuNPs was evaluated via fluorescent analysis of TAMRA-aptamer in the presence of nanomaterials. As illustrated in Fig. 4A, the TAMRA-aptamer was adsorbed onto the GO/AuNPs surface by π–π stacking and electrostatic attraction, and then its fluorescence intensity was mostly quenched by GO/AuNPs. However, the fluorescence intensity was less quenched when GO was adsorbed. This result suggested that GO/AuNPs as a hybrid material provides more chances for the interaction between TAMRA-aptamer and GO/AuNPs by enhancing the capture efficiency and stability. Thus, the enhanced quenching effect of GO/AuNPs could make sensitive detection with a high signal-to-background ratio. Next, the only fluorescence intensity quenched TAMRA-aptamer on the surface of GO and GO/AuNPs was analyzed after removing unbound TAMRA-aptamer on the surface of GO by centrifugation (Fig. 4B).

### 3.2. Optimization of analysis conditions

It is known that the concentrations of GO/AuNPs and aptamer are crucial factors for detection analysis [43]. To achieve the best analysis performance, we optimized the concentration GO and GO/AuNPs and the reaction time in the detection system using 20 nM of TAMRA-aptamer (Supplementary information, Fig. S1). The relative fluorescence intensity ($F/F_0 - 1$) increased constantly at the concentrations of GO and GO/AuNPs up to 0.2 mg/mL. Using $F_0$ and $F$ as references, the fluorescence intensity of the TAMRA-aptamer at 520 nm was measured with or without GO and GO/AuNPs. It was confirmed that over 90% fluorescence intensity of the TAMRA-aptamer was efficiently quenched by GO/AuNPs at concentration above 0.18 mg/mL. Furthermore, it implied that the interaction of TAMRA-aptamer with GO/AuNPs should have been more effective than that with GO. However, the concentrations above 0.2 mg/mL inhibited the target reaction due to the excessive amount of particles. Thus, we choose the optimum concentration at 0.18 mg/mL. This concentration of GO/AuNPs provided the highest efficiency, and took advantage of the detection system.

To identify the optimal analysis time, the quenching time for GO and GO/AuNPs–TAMRA-aptamer complexes was confirmed by monitoring the fluorescence intensity ratios ($F/F_0$) for 40 min with 5 min interval. After addition of 0.18 mg/mL of GO or GO/AuNPs to 20 nM TAMRA-aptamer solution, the fluorescence of TAMRA-aptamer was immediately quenched upon adsorbing onto the GO surface (Fig. S1 in Supplementary information). Over 90% reduction of the fluorescence intensity of the TAMRA-aptamer was obtained by addition of GO/AuNPs (0.18 mg/mL) for 15 min incubation. This result indicates the strong quenching effect of GO/AuNPs against the fluorescence of the TAMRA-aptamer. Thus, the followed experiments were performed by the concentration of 0.18 mg/mL and 15 min reaction time.

### 3.3. Cell viability

To examine the cytotoxicity of GO/AuNPs before the target detection, MTT assay was performed using SKOV3 and MCF-7 cells treated with two kinds of particles for 24 h (Fig. S2 in

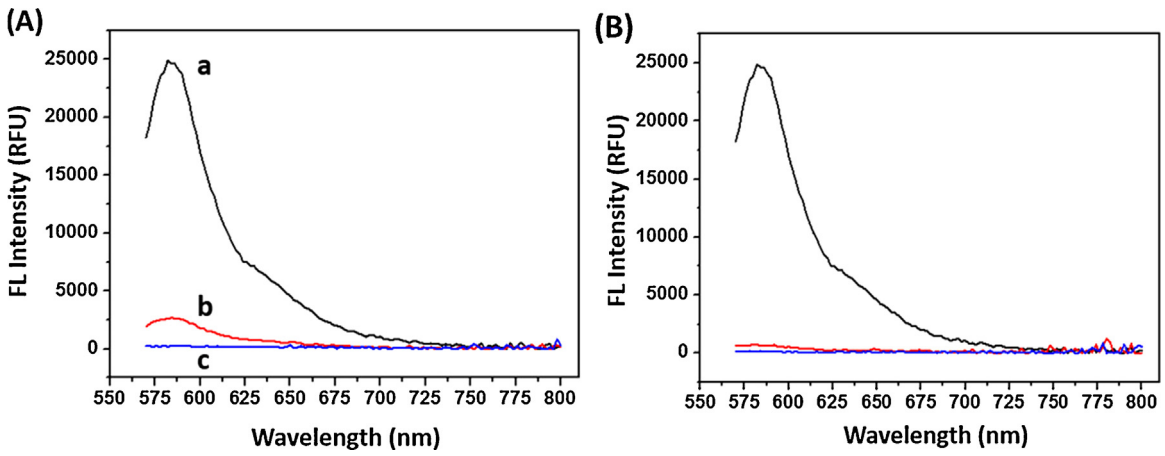


**Fig. 4.** (A) Fluorescence emission spectra of TAMRA-aptamer (20 nM) under different conditions: (a) TAMRA-aptamer, (b) TAMRA-aptamer + GO (0.18 mg/mL) and (c) TAMRA-aptamer + GO/AuNPs (0.18 mg/mL). (B) Fluorescence emission spectra of TAMRA-aptamer + GO and TAMRA-aptamer + GO/AuNPs after centrifugation for relative comparison. Excitation: 545 nm, and emission: 580 nm.

Supplementary information). Both cells showed similar viability loss in dose-dependent effects of GO and GO/AuNPs. Even at the highest concentration of 0.20 mg/mL, about 80% and 67% of the cell viability remained by treatment of GO and GO/AuNPs, respectively. The viability loss triggered by GO/AuNPs than GO may be exacerbated by the AuNPs on GO sheets because the chemically synthesized AuNPs have some toxicity [45]. Thus, more studies are needed to ameliorate the cell toxicity of GO/AuNPs.

### 3.4. Target detection

In order to assess the detection ability of GO/AuNPs, the HA-binding domain of CD44 was used as the target. Fig. 5 shows the fluorescence histogram between GO and GO/AuNPs–TAMRA-aptamer complexes upon incubation with different concentrations of CD44 target. In Fig. 5A, the fluorescence intensities of GO and GO/AuNPs–TAMRA-aptamer complexes were steadily increased at target concentrations in range of $1 \times 10^3 \sim 1 \times 10^5$ CFU/mL. At the case of concentrations above $1 \times 10^6$ CFU/mL, the intensities were sharply increased with GO/AuNPs–TAMRA-aptamer complex, while only slight increase was observed with GO–TAMRA-aptamer complex. Furthermore, a linear correlation was observed between $F - F_0$ and target concentrations with linear equations of $Y = 312.09X - 275.71$ (regression coefficient $R^2 = 0.956$) and $Y = 521.2X - 616$ (regression coefficient $R^2 = 0.9474$) for GO and GO/AuNPs–TAMRA aptamer complexes, respectively (Fig. 5B). Specifically, the limit of detection (LOD) of target equals to $1 \times 10^1$ CFU/mL based on $3\sigma$/slope, where $\sigma$ is the standard deviation of the blank. With increasing $CD44^+$ target cells, however, the fluorescence intensity based on GO/AuNPs was much higher than that of the fluorescent based on GO. This result is the fluorescence arising after the binding between GO/AuNPs–TAMRA aptamer complex and the target. The fluorescence quenching ability of GO has been well evaluated in many studies [21,46,47]. Furthermore, the binding between nanomaterials and ssDNA increases electrostatic repulsion and keeps the quenching efficiencies [46]. The synergistic effect from simultaneous fluorescence quenching using GO and AuNPs may give a higher fluorescence intensity compared to GO [32–35,46]. Therefore, these noticeable differences of fluorescence intensity based on GO/AuNPs facilitate more accurate and sensitive detection.

The variation in fluorescence intensity between GO and GO/AuNPs–TAMRA-aptamer complexes upon hybridization with a CD44 target cell was examined by flow cytometry. The degree of reactivity of the TAMRA-aptamer complexes with target cells could be quantified by determining the fluorescence emission (Fig. S3 in Supplementary information). The target cells readily engulfed GO and GO/AuNPs–TAMRA-aptamers and it was demonstrated by increased fluorescence upon reaction of target cells with the TAMRA-aptamers compared untreated controls. Cellular uptake was much more profound with the GO/AuNPs–TAMRA-aptamer compared to the GO–TAMRA-aptamer. These results indicate that GO/AuNPs–TAMRA-aptamer complexes can enhance fluorescence intensity since GO/AuNPs were highly quenched with the fluorescence dye.

Fluorescence microscopy was applied to further confirm the effects on the target. Target cells were incubated with GO and GO/AuNPs–TAMRA-aptamer complexes for 1 h at 37 °C (Fig. 6). We observed brighter fluorescence with the GO/AuNPs–TAMRA-aptamer complex, indicating high quenching and increased uptake of the complex by target cells. In contrast to the TAMRA-aptamer binding to $CD44^+$ cells, none of TAMRA-aptamers bound to $CD44^-$ MCF-7 cells (Fig. S4 in Supplementary information). These results reveal that the proposed detection assay based on GO/AuNPs exhibits high sensitivity and ease of use for targeting or imaging agent due to the function as great enhancers of signal-to-background ratio.

For specificity of the fluorescence sensing strategy, parallel experiments were performed to evaluate the specificity through CD44 negative target cells such as MCF-7 breast cancer cells and A549 lung cancer cells. The $CD44^-$-cells and other $CD44^+$ target cells, including SKOV3 ovarian carcinoma cells, T98G brain cancer cells, and MDA-MB-231 breast cancer cells, were investigated under the same experimental conditions ($1 \times 10^6$ CFU/mL) to analyze the specificity of the method. As shown in Fig. 7, the results indicated that CD44 positive target cells noticeably increased the fluorescence. On the other hands, fluorescence recovery was weakly observed in MCF-7 and A549 CD44 negative cells. Especially, the fluorescence enhancement in the presence of SKOV3, T98G, and MDA-MB-231 target cells with GO/AuNPs–TAMRA-aptamer complexes was almost 7-fold than negative cells. These results definitely indicated that the suggested fluorescence detection system has good specificity, which can make a distinction target cell and non-target cell. Moreover, the sensing platform based on GO/AuNPs can make the target detection more precise and clear compared to GO-based platform.

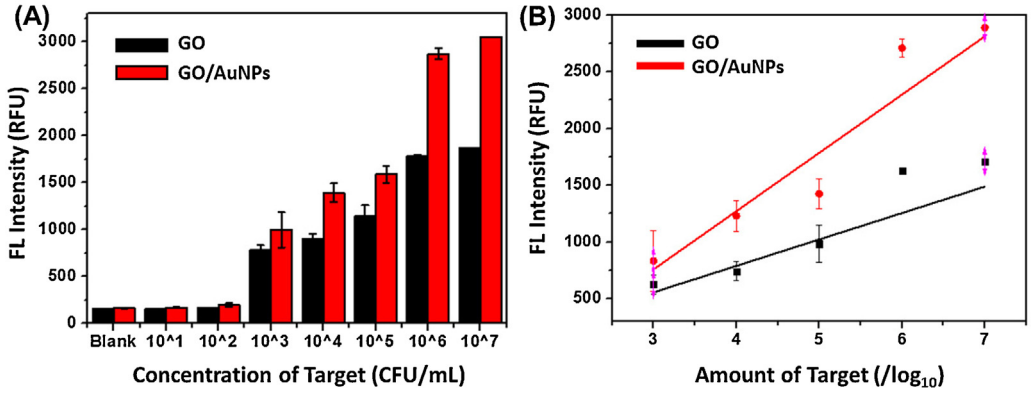


**Fig. 5.** (A) Fluorescence emission histogram of the hybrid of GO and GO/AuNPs–TAMRA-aptamer complexes and different concentrations of target cells (Blank, $10^1$, $10^2$, $10^3$, $10^4$, $10^5$, $10^6$, $10^7$ CFU/mL). (B) The calibration plot of fluorescence intensity against the concentration of target cells. Conditions: TAMRA-aptamer concentration: 20 nM, GO and GO/AuNPs concentration: 0.18 mg/mL, Excitation: 545 nm, and emission: 580 nm. Error bars indicate standard deviation ($n = 3$).

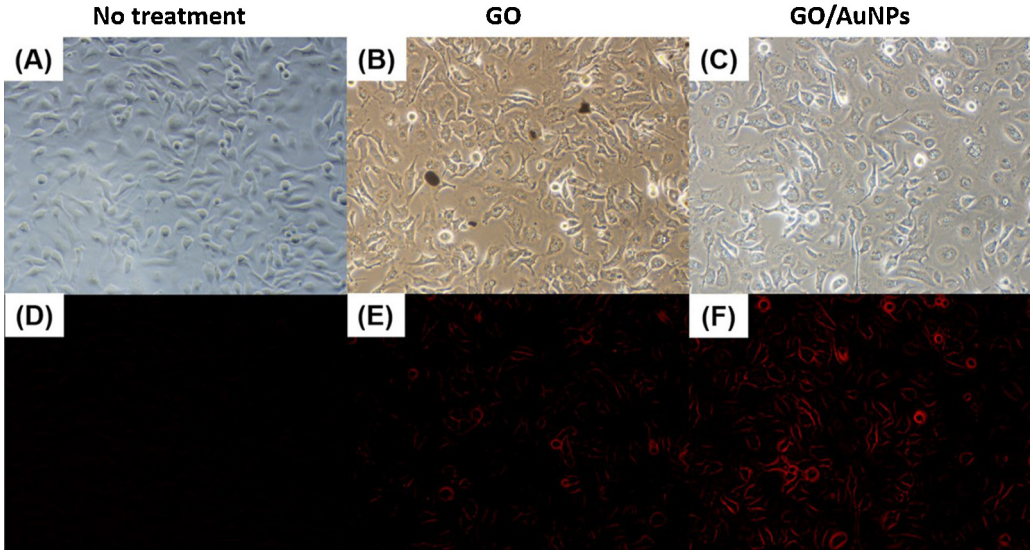


**Fig. 6.** Fluorescence microscope images of unreacted and reacted GO–TAMRA aptamer complexes and GO/AuNPs–TAMRA aptamer complexes on $CD44^+$ SKOV3 cell line. (A–C) Differential interference contrast (DIC) images of $CD44^+$ SKOV3 cell line and (D–F) corresponding fluorescence images, respectively. The magnification for all images is 20×. Target cell concentration: $1 \times 10^6$ CFU/mL; TAMRA-aptamer concentration: 20 nM; GO and GO/AuNP concentration: 0.18 mg/mL.

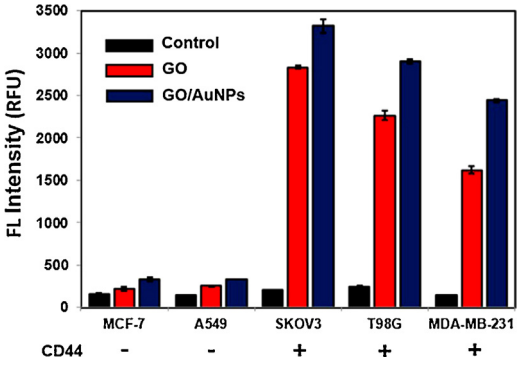


**Fig. 7.** Fluorescence intensities of different target cells reacted with control (no treatment), GO, and GO/AuNPs–TAMRA aptamer complexes. Target cell concentration, $1 \times 10^6$ CFU/mL; TAMRA-aptamer concentration, 20 nM; GO and GO/AuNPs concentration, 0.18 mg/mL (mean ± SD, $n = 3$).

## 4. Conclusions

In summary, we have developed a GO/AuNPs-based fluorescence aptasensor for use as a highly sensitive, selective, and simple detection system. Graphene-based AuNPs prepared with molecular-level dispersion have been used as a capture substance of ssDNA and a quencher for fluorophore to enhance the signal-to-background ratio. GO/AuNPs exhibited the higher sensitivity and specificity for the fluorescent detection of CD44 than those of GO alone due to their structural stability and enhancement of quenching efficiency. Consequently, GO/AuNPs-based fluorescence sensing platform can be used widely to detect other crucial targets such as pathogens and cancer biomarkers.

## Acknowledgements

This study was supported by the Advanced Production Technology Development Program, Ministry of Agriculture, Food and Rural Affairs (312066-3), and the IT R&D program of MoTIE/MISP/KEIT (10044580, Korea).

## Appendix A. Supplementary data

Supplementary data associated with this article can be found, in the online version, at http://dx.doi.org/10.1016/j.colsurfb.2015.07.083

## References


[1] H. Sharma, R. Mutharasan, Review of biosensors for foodborne pathogens and toxins, Sens. Actuators B-Chem. 183 (2013) 535–549.
[2] Y. Huang, X. Chen, N. Duan, S. Wu, Z. Wang, X. Wei, Y. Wang, Selection and characterization of DNA aptamers against *Staphylococcus aureus* enterotoxin C1, Food Chem. 166 (2015) 623–629.
[3] M. Farré, D. Barceló, Toxicity testing of wastewater and sewage sludge by biosensors, bioassays and chemical analysis, TrAC Trends Anal. Chem. 22 (2003) 299–310.
[4] H. Qiu, N. Wu, Y. Zheng, M. Chen, S. Weng, Y. Chen, X. Lin, A robust and versatile signal-on fluorescence sensing strategy based on SYBR green I dye and graphene oxide, Int. J. Nanomed. 10 (2015) 147–156.
[5] X. Xiang, M. Luo, L. Shi, X. Ji, Z. He, Droplet-based mocroscale colorimetric biosensor for multiplexed DNA analysis via a graphene nanoprobe, Anal. Chim. Acta 751 (2012) 155–160.
[6] J. Wang, Electrochemical nucleic acid biosensors, Anal. Chim. Acta 469 (2002) 63–71.
[7] N.S. Eum, D.E. Kim, S.H. Yeom, B.H. Kang, K.J. Kim, C.S. Park, S.W. Kang, Variable wavelength surface plasmon resonance (SPR) in biosensing, Biosystems 98 (2009) 51–55.
[8] Z. Ge, M. Lin, P. Wang, H. Pei, J. Yan, J. Shi, Q. Huang, D. He, C. Fan, X. Zuo, Hybridization chain reaction amplification of microRNA detection with a tetrahedral DNA nanostructure-based electrochemical biosensor, Anal. Chem. 86 (2014) 2124–2130.
[9] J.J. Xu, W.W. Zhao, S. Song, C. Fan, H.Y. Chen, Functional nanoprobes for ultrasensitive detection of biomolecules: an update, Chem. Soc. Rev. 43 (2014) 1601–1611.
[10] Z. Song, Y. Hong, R.T.K. Kwok, J.W.Y. Lam, B. Liu, B.Z. Tang, A dual-mode fluorescence turn-on biosensor based on an aggregation-induced emission luminogen, J. Mater. Chem. B 2 (2014) 1717–1723.
[11] X. Lu, X. Dong, K. Zhang, X. Han, X. Fang, Y. Zhang, A gold nanorods-based fluorescent biosensor for the detection of hepatitis B virus DNA based on fluorescence resonance energy transfer, Analyst 138 (2013) 642–650.
[12] T.A. Feagin, D.P.V. Olsen, Z.C. Headman, J.M. Heemstra, High-throughput enantiopurity analysis using enantiomeric DNA-based sensors, J. Am. Chem. Soc. 137 (2015) 4198–4206.
[13] R. Hu, T. Liu, X.-B. Zhang, S.-Y. Huan, C. Wu, T. Fu, W. Tan, Multicolor fluorescence biosensor for multiplexed detection of DNA, Anal. Chem. 86 (2014) 5009–5016.
[14] Y.F. Duan, Y. Ning, Y. Song, L. Deng, Fluorescent aptasensor for the determination of *Salmonella typhimurium* based on a graphene oxide platform, Microchim. Acta 181 (2014) 647–653.
[15] J.H. Jung, D.S. Cheon, F. Liu, K.B. Lee, T.S. Seo, A graphene oxide based immune-biosensor for pathogen detection, Angew. Chem. Int. Ed. 49 (2010) 5708–5711.
[16] R.C. Huang, W.J. Chiu, Y.J. Li, C.C. Huang, Detection of microRNA in tumor cells using exonuclease III and graphene oxide-regulated signal amplification, ACS Appl. Mater. Interfaces 6 (2014) 21780–21787.
[17] G. Lu, H. Li, C. Liusman, Z. Yin, S. Wu, H. Zhang, Surface enhanced Raman scattering of Ag or Au nanoparticle-decorated reduced graphene oxide for detection of aromatic molecules, Chem. Sci. 2 (2011) 1817–1821.
[18] F. Li, Y. Feng, C. Zhao, P. Li, B. Tang, A sensitive graphene oxide-DNA based sensing platform for fluorescence turn-on detection of bleomycin, Chem. Commun. 48 (2012) 127–129.
[19] J.H. Jung, D.S. Cheon, F. Liu, K.B. Lee, T.S. Seo, A graphene oxide based immune-biosensor for pathogen detection, Angew. Chem. Int. Ed. 49 (2010) 5708–5711.
[20] X.H. Zhao, Q.J. Ma, X.X. Wu, X. Zhu, Graphene oxide-based biosensor for sensitive fluorescence detection of DNA based an exonuclease III-aided signal amplification, Anal. Chim. Acta 727 (2012) 67–70.
[21] S. He, B. Song, D. Li, C. Zhu, W. Qi, Y. Wen, L. Wang, S. Song, H. Fang, C. Fan, A graphene nanoprobe for rapid, sensitive, and multicolor fluorescent DNA analysis, Adv. Funct. Mater. 20 (2010) 453–459.
[22] M. Uddin, T. Kuila, G. Nayak, N. Kim, B. Ku, J. Lee, Effects of various surfactants on the dispersion stability and electrical conductivity of surface modified graphene, J. Alloys Compd. 562 (2013) 134–142.
[23] L. Chen, H. Xie, Properties of carbon nanotube nanofluids stabilized by cationic gemini surfactant, Thermochim. Acta 506 (2010) 62–66.
[24] S. Guo, D. Wen, Y. Zhai, S. Dong, E. Wang, Platinum nanoparticle ensemble-on-graphene hybrid nanosheet: one-pot, rapid synthesis, and used as new electrode material for electrochemical sensing, ACS Nano 4 (2010) 3959–3968.
[25] P.T. Yin, S. Shah, M. Chhowalla, K.-B. Lee, Design, synthesis, and characterization of graphene-nanoparticle hybrid materials for bioapplications, Chem. Rev. 115 (2015) 2483–2531.
[26] K.M.L.T. Pashow, J.D. Rocca, R.C. Huxford, W. Lin, Hybrid nanomaterials for biomedical applications, Chem. Commun. 46 (2010) 5832–5849.
[27] W.-P. Xu, L.-C. Zhang, J.-P. Li, Y. Lu, H.-H. Li, Y.-Y. Ma, W.-D. Wang, S.-H. Yu, Facile synthesis of silver@graphene oxide nanocomposites and their enhanced antibacterial properties, J. Mater. Chem. 21 (2011) 4593–4597.
[28] M.Z. Zhou, G.D. Xia, J. Li, L. Chai, L.J. Zhou, Analysis of factors influencing thermal conductivity and viscosity in different kinds of surfactant solutions, Exp. Therm. Fluid Sci. 36 (2012) 22–29.
[29] N. Halas, Nanoscience under glass: the versatile chemistry of silica nanostructures, ACS Nano 2 (2008) 179–183.
[30] H. Li, L. Rothberg, Colorimetric detection of DNA sequences based on electrostatic interactions with unmodified gold nanoparticles, Proc. Natl. Acad. Sci. U. S. A. 101 (2004) 14036–14093.
[31] D.A. Giljohann, D.S. Seferos, W.L. Daniel, M.D. Massich, P.C. Pate, C.A. Mirkin, Gold nanoparticles for biology and medicine, Angew. Chem. Int. Ed. 49 (2010) 3280–3294.
[32] G. Goncalves, P.A.A.P. Marques, C.M. Granadeiro, H.I.S. Nogueira, M.K. Singh, J. Gracio, Surface modification of graphene nanosheets with gold nanoparticles: the role of oxygen moieties at graphene surface on gold nucleation and growth, Chem. Mater. 21 (2009) 4796–4802.
[33] M. Tang, X. Wang, F. Wu, Y. Liu, S. Zhang, X. Pang, X. Li, H. Qiu, Au nanoparticle/graphene oxide hybrids as stabilizers for pickering emulsions and Au nanoparticle/graphene oxide@polystyrene microspheres, Carbon 71 (2014) 238–248.
[34] T.A. Pham, B.C. Choi, K.T. Lim, Y.T. Jeong, A simple approach for immobilization of gold nanoparticles on graphene oxide sheets by covalent bonding, Appl. Surf. Sci. 257 (2011) 3350–3357.
[35] X. Fu, T. Lou, Z. Chen, M. Lin, W. Feng, L. Chen, Turn-on fluorescence detection of lead ions based on accelerated leaching of gold nanoparticles on the surface of graphene, ACS Appl. Mater. Interfaces 4 (2012) 1080–1086.
[36] E.K. Lim, H.O. Kim, E.J. Jang, J. Park, K.Y. Kim, J.S. Suh, Y.M. Huh, S.J. Haam, Hyaluronan-modified magnetic nanoclusters for detection of CD44-overexpressing breast cancer by MR imaging, Biomaterials 32 (2011) 7941–7950.
[37] A. Somasunderam, V. Thiviyanathan, T. Tanaka, X. Li, M. Neerathilingam, G.L.R. Lokesh, A. Mann, Y. Peng, M. Ferrari, J. Klostergaard, D.G. Gorenstein, Combinatorial selection of DNA thioaptamers targeted to the HA binding domain of human CD44, Biochemistry 49 (2010) 9106–9112.
[38] H. Harada, T. Nakata, Y.H. Takahata, I. Tanaka, M. Nakajima, M. Takahashi, F-16438s, novel binding inhibitors of CD44 and hyaluronic acid, J. Antibiot. 59 (2006) 770–776.
[39] F. Li, J. Zhang, X. Cao, L. Wang, D. Li, S. Song, B. Ye, C. Fan, Adenosine detection by using gold nanoparticles and designed aptamer sequences, Analyst 134 (2009) 1355–1360.
[40] J. Iida, R. Clancy, J. Dorchak, R.I. Somiari, S. Somiari, M.L. Cutler, R.J. Mural, C.D. Shriver, DNA aptamers against exon v10 of CD44 inhibit breast cancer cell migration, PLoS One 9 (2014) e88712.
[41] W.S. Hummers, R.E. Offeman, Preparation of graphitic oxide, J. Am. Chem. Soc. 80 (1958) 1339.
[42] D.C. Marcano, D.V. Kosynkin, J.M. Berlin, A. Sinitskii, Z. Sun, A. Slesarev, L.B. Alemany, W. Lu, J.M. Tour, Improved synthesis of graphene oxide, ACS Nano 4 (2010) 4806.
[43] Y. Wang, Z. Li, D. Hu, C.T. Lin, J. Li, Y. Lin, Aptamer/graphene oxide nanocomplex for in situ molecular probing in living cells, J. Am. Chem. Soc. 132 (2010) 9274–9276.
[44] J. Liu, Y. Li, Y. Li, J. Li, Z. Deng, Noncovalent DNA decorations of graphene oxide and reduced graphene oxide toward water-soluble metal-carbon hybrid nanostructures *via* self-assembly, J. Mater. Chem. 20 (2010) 900–906.
[45] R.K. Das, N. Gogoi, U. Bora, Green synthesis of gold nanoparticles using *Nyctanthes arbortristis* flower extract, Bioproc. Biosyst. Eng. 34 (2011) 615–619.
[46] F. Li, H. Pei, L. Wang, J. Lu, J. Gao, B. Jiang, X. Zhao, C. Fan, Nanomaterial-based fluorescent DNA analysis: a comparative study of the quenching effects of graphene oxide, carbon nanotubes, and gold nanoparticles, Adv. Func. Mater. 23 (2013) 4140–4148.
[47] R.S. Swathi, K.L. Sebastian, Resonance energy transfer from a dye molecule to graphene, J. Chem. Phys. 129 (2008) 054703.